

Design and Implementation of a Hybrid UAV With Model-Based Flight Capabilities

Yijie Ke , Kangli Wang, and Ben M. Chen, *Fellow, IEEE*

Abstract—Hybrid UAV is an attractive design concept in the last decade for its superiority in combining vertical takeoff and landing (VTOL) and cruise flight capabilities. In this paper, we present a systematic design methodology from bottom up for an innovative tail-sitter UAV platform, named J-Lion. Implementation details are included with all design considerations and tradeoffs. All subsystem dynamics is investigated to constitute the dynamics model with a unified form for full envelope. Model-based VTOL and full envelope flights are realized with the obtained dynamics model and sophisticated flight control techniques. Experiment results successfully prove the effectiveness of our design concept and methodology.

Index Terms—Dynamics modeling, hybrid UAV, system design, tail-sitter, unmanned aerial vehicle, vertical takeoff and landing (VTOL).

NOMENCLATURE

ω_i	Rotating speed of two propellers, $i = 1, 2$.
ω_{si}, ω_{ri}	Steady and reference rotating speed of two propellers, $i = 1, 2$.
ρ	Air density.
τ	Time constant for rotor dynamic response.
Ω_b	Angular speed vector of the platform expressed in the body frame, $\Omega_b = (p, q, r)^T$.
F_{aero}	Aerodynamic force vector expressed in the inertial frame.
$F_{surface}$	Force vector from the control surfaces and fins expressed in the inertial frame.
I_f	Moment of inertia matrix in diagonal form, $I_f = \text{diag}(I_x, I_y, I_z)$.
M_{aero}	Aerodynamic torque vector expressed in the body frame.
$M_{prop-gyro}$	Gyroscopic torque vector from the rotating propellers expressed in the body frame.
M_{prop}	Torque vector from the rotating propellers expressed in the body frame.
$M_{surface}$	Torque vector from the control surfaces expressed in the body frame.

$M_{vectorT}$	Torque vector from the vectoring thrust mechanism expressed in the body frame.
q	Quaternion vector.
R_{BE}	Rotation matrix from the body frame to the inertial frame.
R_{RB}	Rotation matrix from the rotor frame to the body frame.
A_{prop}	Area of the propeller actuator disk.
a_q, b_q	Fitting coefficients for propeller torque.
a_t, b_t	Fitting coefficients for propeller thrust.
a_w, b_w, c_w	Fitting coefficients for propeller rotating speed.
C_T	Propeller thrust coefficient in high speed flight.
D_{prop}	Propeller diameter.
g	Gravity acceleration.
m	Platform mass.
M_{propi}	Propeller torque, $i = 1, 2$.
n	Propeller revolution per second.
p_1, p_2	Fitting coefficients for propeller thrust coefficient in high speed flight.
T_{propi}	Propeller thrust, $i = 1, 2$.
throttle $_i$	Throttle input for two propellers, $i = 1, 2$.
V_∞	Propeller advance speed.

I. INTRODUCTION

UNMANNED aerial vehicle (UAV) design has been a persistent topic in the past few decades to fill the increasing requirement shortfalls raised by various application scenarios, such as search and rescue, surveillance, and landscape mapping. A variety of UAVs have been developed, weighing from a few grams to several tons, with the emergence of smart materials, miniature electronics, aerodynamic analysis methods, and advanced flight control algorithms. In terms of aircraft platform structures, they can be categorized into four types: first, fixed-wing; second, rotorcraft; third, flapping wing; and fourth, hybrid UAVs. The hybrid UAV, featured by its superiority in combining both VTOL and cruise flight capabilities, is a promising enabler for missions with constrained takeoff/landing facilities and long flight range requirement.

With above background, we aim to develop a hybrid UAV platform from bottom up. In existing work from the literature, various designs have been proposed, including tilt-rotor design [1]–[5], tilt-wing design [6]–[8], tail-sitter design [9]–[13], and multirotor fixed-wing design [14]–[16]. The tail-sitter configuration is favored in our work for its mechanical simplicity, as it does not require extra tilting mechanisms for wings and rotors,

Manuscript received May 2, 2017; revised September 13, 2017 and January 22, 2018; accepted March 19, 2018. Date of publication March 28, 2018; date of current version June 12, 2018. Recommended by Technical Editor Y. Shi. (*Corresponding author: Yijie Ke.*)

The authors are with the Department of Electrical & Computer Engineering, National University of Singapore, Singapore 117583 (e-mail: keyijie@u.nus.edu; wangkangli@u.nus.edu; bmchen@nus.edu.sg).

Color versions of one or more of the figures in this paper are available online at <http://ieeexplore.ieee.org>.

Digital Object Identifier 10.1109/TMECH.2018.2820222

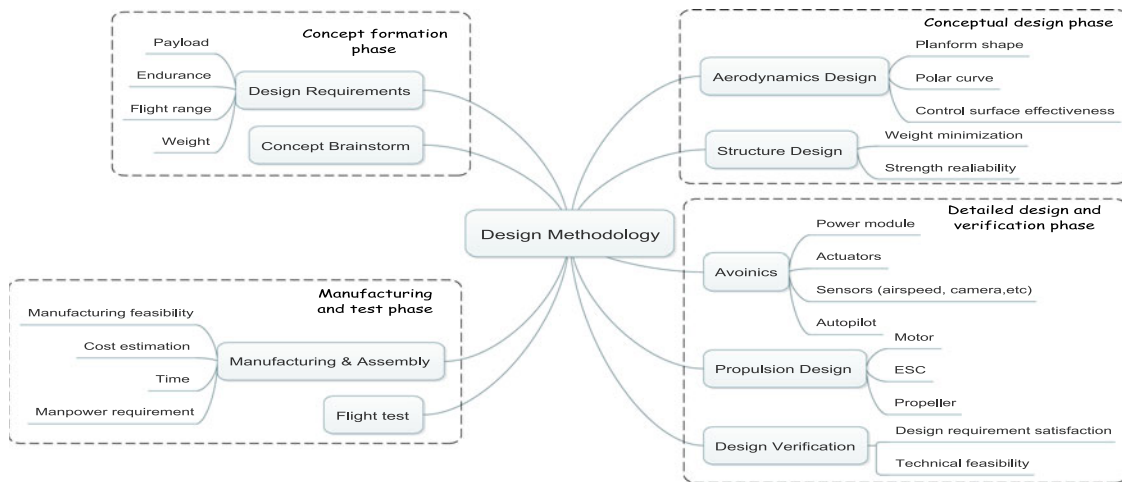


Fig. 1. Design methodology overview.

and its single propulsion system can suffice the need for multiple flight modes.

Our work on the hybrid UAV J-Lion is first featured by its platform design to be presented. One key challenge for the tail-sitter UAV is the compromise between VTOL and cruise flights, hence the existing methodologies originating from those for large aircraft (e.g., [17], [18]) cannot be directly applied. Specifically, the aerodynamic optimization for the full envelope is critical in enhancing the maneuverability in transition phase and increasing payload capability. In [9], a multidisciplinary optimization method was presented to numerically optimize a T-wing platform with several parameters using sequential quadratic programming; their results are not conclusive in the design guidelines, and the T-wing configuration focuses more on the VTOL mode. Kubo and Suzuki [10] introduced a twin-body tail-sitter, but the design procedure was not given and their tail-sitter relies on runways for takeoff and landing although the transitional flight is realized. In [11] and [19], a systematic design methodology was proposed for propulsion system, weight consideration, and UAV configuration, but no successful flight result can be found afterward. Two close commercial examples to our work are the platforms from Google Project Wing [13] and Wingtra [20], but the design details are not disclosed to public. In comparison with our previous work in [21], aerodynamic optimization is pursued particularly in J-Lion development for the full envelope, and enhanced maneuverability is also achieved with sophisticated actuator design and allocation, especially in the VTOL mode under wind disturbance. For the other tail-sitter examples in the literature (see e.g., [12], [22]), little emphasis is placed for the platform design and optimization. In this sense, we endeavor to investigate a systematic design approach that can fulfill the different design requirements in full envelope, which will greatly reduce the development cycle of such hybrid UAVs.

In terms of flight control, the difficulties of transition control for tail-sitter UAVs have long been perceived by researchers [22], [10], and [23] due to its high dynamics uncertainty. Some theoretical work proposed methods under the

optimization framework by solving objective functions with dynamics and envelope constraints offline [24], [25], but those methods cannot be implemented easily due to model uncertainties and onboard computation burden. Typical examples with experiment results adopt either nonlinear dynamic inversion approaches relying on high fidelity experiment data [26], [27], or trivial linear control methods for light weight platforms [28], [29]. In contrast with existing work, our method to be presented alleviates the need for wind tunnel test in [27] and trivial experiment tests in [26], [28], and [29]. The proposed control structure is easy to be implemented, and comparable attitude tracking performance can be achieved by referring to available experiment data in [21] and [27].

The outline of the remaining manuscript is as follows: Section II presents the design methodology and details of our platform; Section III gives a unified full-envelope dynamics model; the model-based controllers for VTOL, transition and cruise flights are described in Section IV; experiment results of VTOL and full envelope flights are given in Section V to prove the design concept and verify our model-based control techniques; finally, we draw some concluding remarks in Section VI.

II. PLATFORM DESIGN

A. Design Methodology

The design methodology shown in Fig. 1 details the procedures and tradeoffs in our design considerations. The design cycle can be divided into four phases as follows.

- 1) *Concept formation:* Design requirements are synthesized for application scenarios, including payload, endurance, flight range, and weight estimation. Concept brainstorm usually comprises the guidelines for hardware and software design, and the criteria for tradeoffs between conflicting factors such as cost and performance.
- 2) *Conceptual design:* We emphasize on propulsion and aerodynamics design because these two factors are the keys to determine specifications that meet flight

requirements. The propulsion subsystem should be able to provide sufficient thrust with proper matching of brushless dc motors, electric speed controllers (ESCs), and propellers. The aerodynamics design consists of complete analysis from planform shape sizing to analytical and computational fluid dynamics (CFD) computation for polar curve. Control surface effectiveness should also be considered to ensure controllability in full flight envelope especially in transition process in which aerodynamic lift is not sufficient to balance total weight.

- 3) *Modular design and verification*: Detailed design is carried out for avionics and structure after the overall layout and planform shape are finalized. Modular design is highly preferred for tailorable application requirements. The structure design emphasizes on weight minimization while ensuring strength reliability, so that payload capability can be realized with a certain margin. Design verification is essential to ensure the fulfillment of design requirements and technical feasibility in both hardware and software systems.
- 4) *Manufacturing and test*: Cost effective and feasible manufacturing methods are sought with balancing between time and manpower constraints. The manufacturing method can even change the structure design plan in the detailed design phase. Prototyping is pursued at early stage to correct design defects. Flight tests are essential to prove our design concept and validate the whole system.

B. Aerodynamics Design

For J-Lion, both the fuselage and wings are designed to contribute lift force as much as possible. For small hybrid UAVs, low Reynolds number ($Re < 5 \times 10^5$) aerodynamics effect can lead to abrupt lift force reduction for traditional airfoil design [30], and this is the critical difference in aerodynamics design between small UAVs and large aircraft. The key requirement is to achieve an optimum among the VTOL, transition and cruise flight modes. In the VTOL mode, the center of gravity (CG) is preferred to be low to enhance stability. During the transition, the aerodynamics of platform should be designed to contribute lift force even with low flight speed, which can alleviate the requirement for the propulsion system. In the cruise flight mode, high lift to drag ratio is favored to achieve maximum flight efficiency, and static stability margin should be guaranteed to facilitate flight control system design. In addition, control surfaces should always be able to provide sufficient forces or torques for flight maneuvers in the full flight envelope.

1) *Fuselage and Wing Design*: Fuselage and wings are main components generating aerodynamic lift, so the airfoil selection for them is crucial. The difficulty in this part is that there is no general guideline available for hybrid UAV design, although massive airfoil databases for low Reynolds number aerodynamics have been reported in literature (see e.g., [31]–[33]). In what follows, we propose a guideline for airfoil selection.

- 1) *Fuselage airfoil*: The airfoil should provide high lift during flight with low drag so that the fuselage lift can help increase flight efficiency; it should exhibit a mild stall

TABLE I
AIRFOIL SELECTION FOR J-LION

Part name	Airfoil	Operating Reynolds number Re	Lift coefficient C_L
Fuselage	SA7038	Around 6.6×10^5	1.4 when AOA= 10°
Wing	NACA 2412	Around 3×10^5	1.2 when AOA= 10°

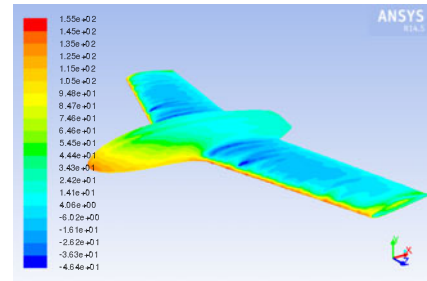


Fig. 2. Total pressure contour for condition with 15-m/s speed and 5° AOA.

characteristic especially in high angle of attack (AOA) condition to assist smooth transition; it is required to have a minimal airfoil thickness to provide sufficient space for onboard electronics system.

- 2) *Wing airfoil*: The airfoil should be with a relatively low camber value because high cambered wings operating under the propeller slipstream will generate a large lateral force that can degrade VTOL stabilization. Tradeoff must be made between low camber and high lift. The airfoil should be able to provide a mild stall characteristic as well.

With proposed guideline above, the planform shape is also finalized after several iterations from balancing weight and aerodynamics, and the selected airfoils are shown in Table I.

2) *Control Surface Sizing*: The sizing of control surfaces can be determined by the flat-plate approximation [34] for required torques. Besides aileron, rudder, and elevator for the cruise flight mode, we adopt extra control surfaces (called fins) in the propeller slipstream to enhance controllability during the VTOL and transition modes. With strong slipstream inflow, these extra control surfaces will provide effective control torques in the full envelope flight.

3) *Computational Results*: We utilize analytical and CFD methods to validate our aerodynamics design. The analytical method is preferred to give a rough estimation of the initial planform size. The CFD method is used in the late phase to refine results for aerodynamic polar curve. The CFD tools we utilize are ANSYS ICEM and Fluent modules. The ICEM module provides powerful automated functions to generate meshes for our J-Lion.

With the generated mesh, the Fluent module is used to compute aerodynamic forces and torques for the speed range 5–20 m/s, and the AOA range 5° – 15° . Fig. 2 shows the static pressure around J-Lion body in the condition of 15-m/s speed and 5° AOA, and it is observed that pressure on the upper

TABLE II
CFD RESULTS FOR J-LION

Case	Speed (m/s)	AOA (deg)	Total lift (N)	Total drag (N)	Fuselage lift (N)	Wing lift (N)	AF position (m)
1	5	5	3.48	0.256	1.02	2.46	0.467
2	5	10	5.51	0.597	1.65	3.86	0.455
3	5	15	5.67	1.27	1.83	3.86	0.471
4	10	5	13.97	1.01	4.11	9.87	0.469
5	10	10	22.22	2.33	6.63	15.60	0.455
6	10	15	22.78	5.00	7.51	15.33	0.468
7	15	5	31.30	2.21	9.23	22.08	0.468
8	15	10	50.68	5.26	15.05	35.65	0.455
9	15	15	56.98	10.78	18.61	38.48	0.458

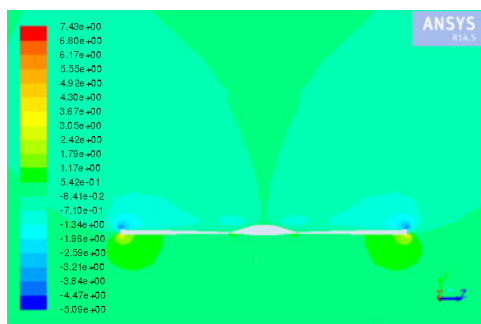


Fig. 3. Spanwise velocity contour for condition with 15-m/s speed and 5° AOA.

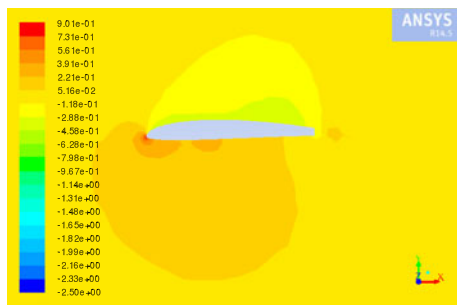


Fig. 4. Pressure coefficient contour for condition with 5-m/s speed and 15° AOA.

surfaces of fuselage and wings is much lower than that on the lower surfaces, indicating a lift force is effectively obtained. The spanwise flow velocity contour is also shown in Fig. 3 which implies that wingtip vortex effect is successfully captured by our computational results.

The partial results for the lift, drag, and aerodynamic focus (AF) position measured from the heading point are summarized in Table II. Note that in the conditions of 15° AOA, our design is able to maintain a lift force with a comparable magnitude to the lower AOA conditions, while conventional design with NACA airfoils tends to degrade the aerodynamic performance greatly due to stall effect. The pressure coefficient contour is shown in Fig. 4 for flight condition with 5-m/s speed and 15° AOA, for which the corresponding lift coefficient is 0.7.

The key features are pointed out below from the obtained results:

- 1) Satisfactory aerodynamic lift can be generated in the speed range 5–20 m/s, and the AOA range 5–15°. The static stability can be guaranteed with the relative location of CG and AF.
- 2) The fuselage contributes about 30% of the total aerodynamics lift in all computed cases. It increases flight efficiency significantly.
- 3) The low Reynolds number aerodynamics effect is successfully handled in low flight speed conditions, which provides enhancement for the transition flight.

C. Structure, Propulsion, and Avionics Design

1) *Structure and Propulsion*: The structure design of J-Lion aims to minimize platform weight and obtain a desired CG position for static stability in the cruise flight. The subtlety in our structure design is that we optimize each part while ensuring its strength. The main materials we choose are carbon fiber and Expanded Polyolefin (EPO) foam. The carbon fiber material is able to build strong body skeletons while EPO foam is used to construct the main body with the required aerodynamic shape. Our structure design solution is proved to be cost-effective and feasible with some very common manufacturing facilities like computer numerical control (CNC) cutting and milling. The estimated weight from computer aided design (CAD) including all components is 2.7 kg, which meets the design requirement in the conceptual design phase.

To enhance maneuverability, we adopt a dual-rotor configuration with vectoring thrust mechanisms. The single degree of freedom vectoring thrust mechanism can provide reliable control authority in full envelope. The propulsion set is determined with the consideration of its maximum thrust and weight. The propeller is usually recommended by the motor datasheet, and it is preferred to be small and with a high pitch value, in order to reduce the airflow disturbance of the wings and balance the performance between VTOL and cruise flights, respectively. Based on the specification of the propulsion set and the drag force from the CFD results, we can estimate the power consumption

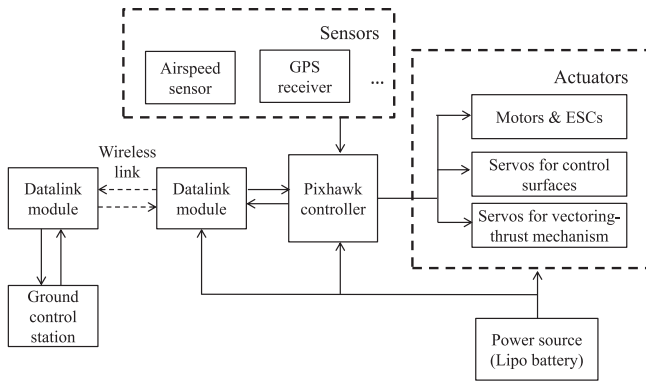


Fig. 5. Avionics schematic for J-Lion.

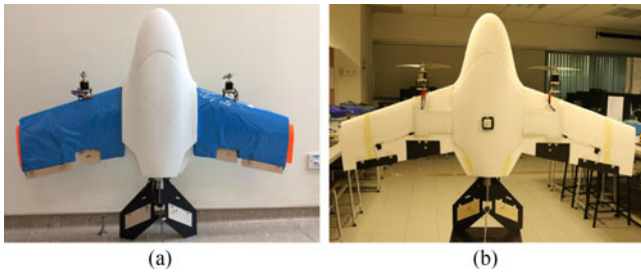


Fig. 6. J-Lion prototypes. (a) J-Lion Prototype 1. (b) J-Lion Prototype 2.

in VTOL and cruise flights, then the battery capacity can be determined to fulfill the need of endurance.

2) *Avionics*: The avionics subsystem of J-Lion is shown in Fig. 5, which includes a flight controller, sensors, and actuators. The onboard system communicates with a ground control station via a datalink for operation commands.

The flight controller we adopt is an open-source Pixhawk autopilot with customized software. The sensors currently used include GPS and airspeed sensor. The GPS sensor provides position information for localization, and the airspeed sensor outputs speed for the cruise flight mode. Other sensors can also be integrated based on application requirements. The actuators include servos for control surfaces, vectoring thrust mechanisms, ESCs, and motors.

D. Prototypes

We have constructed two versions of prototypes during the iterations, which are designed with different manufacturing solutions. Prototype 1 shown in Fig. 6(a) utilizes carbon fiber material for the spar-rib body structure and wing skin, and the carbon cloth skin is covered by plastic wrap. This version requires high assembling skills and thus costs more manpower. Prototype 2 [see Fig. 6(b)] is made of carbon fiber plates, rods, and foams. The foam wings are of lightweight and easy repairability, thus we adopt this version for further research.

The specifications of J-Lion in Prototype 2 are listed in Table III, and the corresponding design points are highlighted for a brief sum up.

- 1) A systematic design methodology is built up to streamline the design flow.

TABLE III
J-LION SPECIFICATIONS

Total weight without payload	2.83 kg
Wingspan	1.5 m
Power	5300mAh Lipo battery
VTOL endurance	about 10 minutes
Cruise flight endurance	about 30 minutes
Cruise flight speed	about 15 m/s

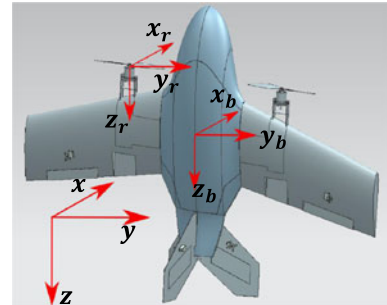


Fig. 7. Coordinate frames.

- 2) Comprehensive aerodynamic design is conducted to achieve an optimized compromise among multiple flight modes.
- 3) Actuator selection and control surface sizing are completed to ensure effective control authority in full envelope.
- 4) Structure design is pursued with utmost care for desired weight layout and economic consideration.

III. DYNAMICS MODELING

In this section, we derive the unified dynamics model structure for J-Lion in full envelope with details on rotor dynamics, vectoring thrust, and control surface dynamics. These actuator dynamics plays an essential role in predicting flight dynamics performance at the early stage from system point of view. As an example, one key consideration in the conceptual design phase is to determine whether the vectoring thrust mechanism and control surfaces can produce sufficient control authority in transition.

A. Unified Model Structure

The unified model structure is derived to describe the full envelop dynamics without switching of coordinate frames. The adoption of this structure can facilitate the build-up of unified flight control software framework.

1) *Coordinate Frames*: Shown in Fig. 7, the global inertial frame (x, y, z) is set to be the NED (north-east-down) frame. The body frame (x_b, y_b, z_b) is defined with its origin located at the CG, and y_b, z_b direction pointing to its wingtip and tail, respectively. The rotor frame (x_r, y_r, z_r) is defined to describe the vectoring thrust direction, and the axes are parallel with the body frame axes when no vectoring thrust angle is applied. The origin of rotor frame is located at the center of vectoring thrust mechanism.

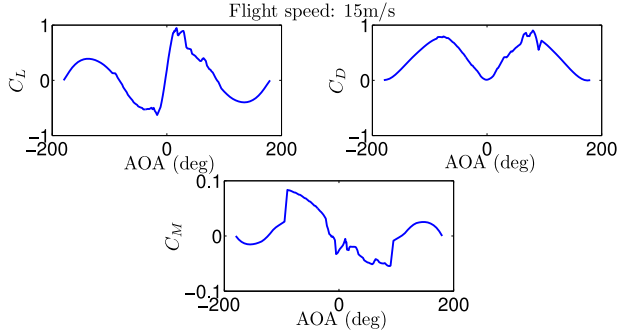


Fig. 8. Aerodynamic coefficients for cruise flight with speed 15 m/s.

2) *Kinematic, Force, and Moment Equations*: To avoid singularity, the kinematic equation can be expressed in either rotation matrix or quaternion as

$$\dot{\mathbf{R}}_{BE} = \mathbf{R}_{BE} \mathbf{\Omega}_R, \quad \dot{\mathbf{q}} = -\frac{1}{2} \mathbf{\Omega}_q \mathbf{q} \quad (1)$$

where $\mathbf{\Omega}_R, \mathbf{\Omega}_q$ are skew symmetric matrices with respect to the angular speed and quaternion vectors.

Let the position be $\mathbf{p} = (x, y, z)^T$, the velocity be $\mathbf{v} = (u, v, w)$, the compact form of the force equation is

$$\dot{\mathbf{p}} = \mathbf{v}$$

$$\dot{\mathbf{v}} = g\mathbf{e}_3 - \frac{1}{m} \mathbf{R}_{BE} \mathbf{R}_{RB} (T_{prop1} + T_{prop2}) \mathbf{e}_3 + \frac{1}{m} \mathbf{F}_{surface} + \frac{1}{m} \mathbf{F}_{aero} \quad (2)$$

where $\mathbf{e}_3 = (0, 0, 1)^T$. The magnitude of $\mathbf{F}_{surface}$ is usually much smaller than others, hence it can be neglected. \mathbf{F}_{aero} is the main term in the force equation during cruise flight. The aerodynamic coefficients for \mathbf{F}_{aero} can be determined by CFD, empirical methods, or flight experiments.

Based on D'Alembert–Lagrange equation, the compact form of the moment equation in the body frame can be formulated as

$$\mathbf{I}_f \dot{\mathbf{\Omega}}_b = -\mathbf{\Omega}_b \times (\mathbf{I}_f \mathbf{\Omega}_b) + \mathbf{M}_{prop-gyro} + \mathbf{M}_{surface} + \mathbf{M}_{prop} + \mathbf{M}_{vectorT} + \mathbf{M}_{aero} \quad (3)$$

where \mathbf{M}_{aero} can be determined with the same methods for \mathbf{F}_{aero} . A typical figure for aerodynamic lift, drag and torque coefficients (C_L, C_D, C_M) in the full flight envelope is shown in Fig. 8, obtained with our first principle modeling method [35]. For different payload, the parameters of mass and moments of inertia are updated accordingly for subsequent control design.

B. Rotor Dynamics

In common practice, rotor dynamics is usually simplified with a steady response model, i.e., only steady thrust and torque are considered. However, the dynamic rotor response actually determines the bandwidth in the actuator layer, hence one necessity lies in the investigation of dynamic rotor behavior to enhance the overall control performance. In addition, the propeller thrust decreases with increasing flight speed. A prediction method for

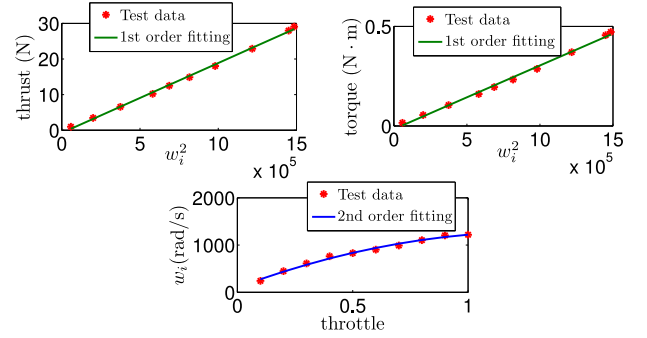


Fig. 9. Steady response results in rotor experiment.

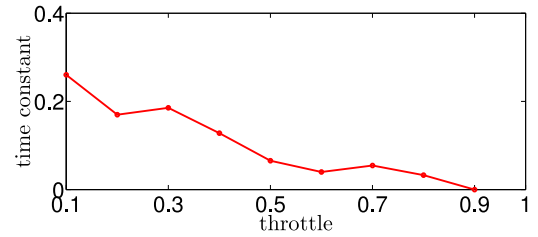


Fig. 10. Time constants for rotor dynamic response.

the thrust with high advance ratio is required to compensate the propeller dynamics model in the high speed operating regime.

1) *Low-Speed Model*: With a series of step throttle input, both steady and transient rotor responses can be captured. The steady response of the rotor dynamics is shown in Fig. 9, wherein the thrust and torque channels resemble a linear relationship with angular speed square value, and the response from the throttle input to its corresponding steady angular speed shows a clear nonlinearity with second-order fitting approximation. The transient response from the throttle input to the angular speed is identified with a first-order approximation and the time constant plot is shown in Fig. 10, indicating that the rotor responds faster with increasing throttle. The low-speed model form is hence given as

$$\omega_{si} = a_w \cdot \text{throttle}_i^2 + b_w \cdot \text{throttle}_i + c_w$$

$$T_{propi} = a_t \cdot \omega_i^2 + b_t, \quad M_{propi} = a_q \cdot \omega_i^2 + b_q$$

$$\omega_i = \frac{1}{\tau_S + 1} \omega_{ri} \quad (4)$$

2) *High-Speed Compensation*: In order to predict the propeller thrust in the cruise flight, high-speed compensation is achieved by constructing a database for the propeller thrust with respect to inflow speed and rotating speed. For the APC propellers employed in our platform, some wind tunnel experiment data can be obtained from the literature (see e.g., [36]), but the shortcoming is that the dataset is usually with limited speed range and cannot be directly used. An alternative is to utilize the APC simulation data from its producer [37], which also provides acceptable accuracy after being verified with wind tunnel experiment data. Hence, we decide to approximate the APC simulation database to compensate the low-speed model in the high speed operating regime. With a first-order approximation

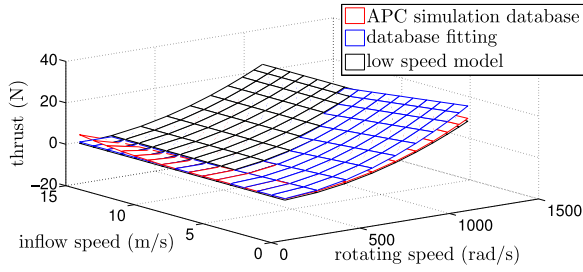


Fig. 11. Comparison of the propeller thrust from the APC simulation database, database fitting, and low-speed model.

between the thrust coefficient and the advance ratio, we can obtain a low order fitting method for the APC simulation database. The comparison of the APC simulation database, database fitting results, and low-speed model for APC 11×5.5 propeller is shown in Fig. 11.

Depending on flight conditions, desired propeller rotation speed can be accurately computed by fitting the simulation database in a specific range. The low-speed model is preferred for flight speed under 8 m/s, and we adopt the database fitting method for the higher speed part. The high speed model form is given as

$$C_T = p_1 J + p_2, \quad T_{\text{prop}} = \rho C_T n^2 D_{\text{prop}}^4 \quad (5)$$

where $J = \frac{V_\infty}{n D_{\text{prop}}}$ is the advance ratio.

C. Vectoring Thrust and Control Surfaces Dynamics

Vectoring thrust and control surfaces produce torques in attitude control, and the torque amplitude and actuation bandwidth are directly related to the performance of actuator. A detailed investigation of the actuator properties can refine the conceptual design at the early stage.

1) **Vectoring Thrust:** The vectoring thrust mechanism driven by a high torque servo is designed to provide pitch torque for the whole flight envelope. The maximum tilting angle can reach 30° , thus sufficient pitch torque can be achieved. It is a spatial four-bar mechanism, and the tilting angle resembles a linear mapping from the servo input. The servo response time is around 0.14 s for 60° rotation angle, which guarantees responsiveness for vectoring thrust actuation. The dynamics of vectoring thrust can be characterized as

$$M_{vT} = T_{\text{prop}} l_{\text{prop}} \sin(\delta_p), \quad \delta_p = k_p u_{\text{servo}} \quad (6)$$

where M_{vT} is the magnitude of the torque produced by the vectoring-thrust propellers, T_{prop} is the propeller thrust, l_{prop} is the arm length from the propeller center to CG, k_p is the scaling factor from servo input to vectoring angle, and u_{servo} is the normalized servo input with range $[-1, 1]$.

2) **Control Surface Dynamics:** The control surfaces employed in J-Lion include the aileron, elevator, rudder and two fins in the slipstream region of the propellers. The control surface dynamics is modeled with a flat-plate approximation, and the corresponding torques can be computed with

$$M_{\text{surf}} = 0.5 \rho C_{L\text{surf}} S_{\text{surf}} l_{\text{surf}} V_{\text{flow}}^2, \quad C_{L\text{surf}} = 2\pi \delta_{\text{surf}} \quad (7)$$

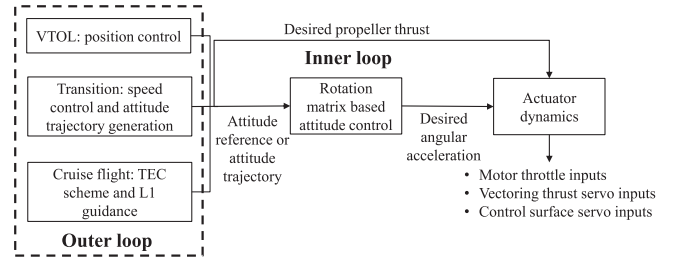


Fig. 12. Control block schematic.

where M_{surf} is the magnitude of torque produced by a control surface, $C_{L\text{surf}}$ is a lift coefficient, l_{surf} is the arm length from the control surface center to CG, and δ_{surf} is the deflection angle of the control surface. The airflow speed V_{flow} for the aileron, elevator, and rudder is simply the relative wind speed along z_b axis. For the fins in the propeller slipstream region, the airflow speed is computed with

$$V_{\text{flow}} = \sqrt{V_\infty^2 + \frac{2T_{\text{prop}}}{\rho A_{\text{prop}}}} \quad (8)$$

IV. MODEL-BASED CONTROL DESIGN

To facilitate the description of our control design, the overall control block is depicted in Fig. 12, which is decomposed into the outer loop, inner loop, and actuator dynamics. The control design is carried out for VTOL, transition and cruise flights separately. The switching between different modes is triggered by the pitch angle reference, for example, the UAV will enter the cruise flight mode during forward transition when the pitch angle reference reaches -70° .

A. VTOL Control Design

The flight performance of the VTOL mode is a key criteria to validate our design methodology. The main idea behind our control design is to apply the aforementioned model in Section III. The model accuracy guarantees the effectiveness and performance of the overall flight control system.

1) **Position Control:** With the position reference provided from a navigation module, the position control module outputs an attitude reference to guide UAV to a desired position or track a certain desired trajectory. The following proportional-integral differential (PID) control law can be applied with limited velocity and acceleration references:

$$\begin{aligned} v_d &= \text{sat}(\mathbf{K}_{p1} e_p, v_{d\text{max}}) \\ a_d &= \text{sat} \left(\mathbf{K}_{p2} e_v + \mathbf{K}_{d2} \frac{d}{dt} e_v + \mathbf{K}_{i2} \int e_v dt, a_{d\text{max}} \right) \end{aligned} \quad (9)$$

where v_d , $v_{d\text{max}}$ are desired velocity and velocity limit, a_d , $a_{d\text{max}}$ are desired acceleration and acceleration limit, e_p , e_v are position error and velocity error, respectively. \mathbf{K}_{p1} , \mathbf{K}_{p2} , \mathbf{K}_{d2} , and \mathbf{K}_{i2} are the PID control gains, and $\text{sat}(x_1, x_2)$ is a saturation function that constrains x_1 within $[-x_2, x_2]$.

To achieve a desired acceleration, the force equation (2) is utilized. By assuming the alignment of thrust vector with the z_b axis, the attitude reference can be obtained. In addition, the tilting angles with respect to x_b, y_b should be explicitly constrained for safety protection because control authority is limited in the roll channel due to thrust limit and delay in the motor response.

For take-off and landing, since the height measurement from the GPS or barometer is not accurate, we set a preset acceleration to launch J-Lion quickly, and the pilot will disarm the autopilot after our platform lands on the ground. Additional sensors like laser pointers will be employed for better landing performance in our future work.

2) *Attitude Control*: Attitude control scheme is currently adopted from rotation-matrix-based methods in [38] and [39], in which desired torque in body axes is obtained with a two-loop control scheme by comparing current attitude with the attitude reference. The noteworthy feature of our work here is that all control gains matrices are computed based on the moment equation given in (3), and required torques in actuator layer are obtained using nonlinear dynamics inversion with explicit subtraction of coupling term and propeller torques. For instance, the desired torque from the fins for VTOL yaw control is computed as

$$M_{\text{fin}} = I_z \dot{r}_d - (I_x - I_y) pq - M_{\text{prop}} \quad (10)$$

where \dot{r}_d is the desired angular acceleration in the yaw channel, M_{prop} is the magnitude of the propeller torque in the yaw channel determined from the rotor low-speed model in Section III-B1. The required fin deflection can then be computed with (7) and (8) in a straightforward way.

B. Transition Control Design

From the lessons gained from flight crashes during development, the transition maneuver cannot be realized without control robustness. The maneuver of forward transition is to transit system form : from VTOL to cruise flight. The requirement is that a cruise speed must be gained in this maneuver to ensure a sufficient aerodynamic lift force, which can be considered as a terminal constraint. Besides, attitude stability must also be guaranteed ; during steady acceleration.

Reversely, the backward transition from cruise flight to VTOL requires the UAV to maintain attitude stability during quick deceleration after maneuvering. Large aerodynamic forces and torques are expected in this process.

1) *Forward Transition*: Inspired by the work in [23] and [24], we decouple the forward transition process into the speed and attitude channels and adopt a maneuver strategy with constant acceleration and pitch rate. Control design for these two channels will be illustrated in the following, and the desired actuator outputs are computed based on model elements in Section III.

a) *Speed Channel*: The speed channel can be approximated as a first-order system with the propeller thrust as the input, and the airspeed as the measurement output. The desired propeller thrust can be obtained with a simple proportional control scheme to guarantee the steady acceleration as

$$T_d = ma_d + mg_{\text{body}} = K_p(V_{\text{ref}} - V_a) + mg_{\text{body}} \quad (11)$$

where a_d is the magnitude of the desired acceleration in the body z_b axis, V_{ref} is the speed reference, V_a is the speed value from the airspeed sensor, K_p is the proportional gain, T_d is the desired thrust from the propellers, and g_{body} is the component of the gravity acceleration in the z_b axis. With the rotor model from Section III-B, the desired thrust from the propellers can be obtained by computing the corresponding desired rotating speed in terms of the airspeed.

b) *Attitude Channel*: Each attitude is approximated as a decoupled second-order system with the desired torques in body axes as the control inputs. Particular emphasis is given to the pitch channel wherein the aerodynamic torque matters most. For yaw and roll channels in the body frame, relatively slow responses are expected due to damping torques and high moments of inertia, so a standard linear control method is applied for stabilization.

1) *Pitch Channel*: In the pitch channel, the vectoring thrust and elevator are activated to provide control torque. Due to the uncertain aerodynamic torque in the forward transition, unexpected oscillations tend to increase the drag force and affect the speed channel. Hence, the pitch trajectory reference has to be smooth and kept within our control authority. Also, robustness should be guaranteed for unknown model dynamics. In what follows, we present a detail procedure for reference generation and a control system design using the robust and perfect tracking (RPT) control technique of [40].

a) *Reference generation*: We employ the method from [41] which solves an optimization problem for a second-order double integrator system with minimum time objective (12). $u_j(t)$ is the decision variable, $v_0, v_{\text{rref}}, a_0$ are terminal constraints, and both $a(t)$ and $u_j(t)$ are bounded.

$$\begin{aligned} \min_{u_j(t), t \in [0, T]} \left\{ J = \int_{t=0}^T dt \right\} \\ \dot{v}(t) = a(t) \\ \dot{a}(t) = u_j(t) \\ v(0) = v_0, v(T) = v_{\text{rref}} \\ a(0) = a_0, a(T) = 0 \\ -u_{j_{\text{max}}} \leq u_j(t) \leq u_{j_{\text{max}}}, \forall t \in [0, T] \end{aligned} \quad (12)$$

With target pitch and pitch rate states, the algorithm is able to generate real-time pitch and pitch rate references θ_r, q_r by switching between acceleration increasing, constant acceleration or acceleration decreasing phases.

b) *RPT control*: Given a linear time-invariant system characterized by

$$\Sigma = \begin{cases} \dot{\mathbf{x}} = A\mathbf{x} + B\mathbf{u} + E\mathbf{w} \\ \mathbf{y} = C_1\mathbf{x} + D_1\mathbf{w} \\ \mathbf{h} = C_2\mathbf{x} + D_2\mathbf{u} + D_{22}\mathbf{w} \end{cases} \quad (13)$$

where $\mathbf{x}, \mathbf{u}, \mathbf{w}, \mathbf{y}$, and \mathbf{h} is the state, control input, disturbance, measurement, and controlled output, respectively, and given any initial condition \mathbf{x}_0 , the RPT control of [40] is to design a control

law of the following form

$$\begin{aligned}\dot{\mathbf{v}} &= A_c(\varepsilon)\mathbf{v} + B_c(\varepsilon)\mathbf{y} + G_0(\varepsilon)r + \dots \\ &\quad + G_{\kappa-1}(\varepsilon)r^{\kappa-1} \\ \mathbf{u} &= C_c(\varepsilon)\mathbf{v} + D_c(\varepsilon)\mathbf{y} + H_0(\varepsilon)r + \dots \\ &\quad + H_{\kappa-1}(\varepsilon)r^{\kappa-1}\end{aligned}\quad (14)$$

where \mathbf{v} is the controller state, r^i , $i = 0, \dots, \kappa - 1$, are the i th order derivative of the reference r , such that when it is applied to the given system, the resulting closed-loop system is asymptotically stable, and the tracking error $e(t, \varepsilon) := h(t, \varepsilon) - r(t)$ has

$$\|e\|_p = \left(\int_0^\infty |e(t)|^p dt\right)^{1/p} \rightarrow 0, \text{ as } \varepsilon \rightarrow 0. \quad (15)$$

Generally, the RPT control law gives excellent tracking performance by feedforwarding the higher order derivative terms of the reference signal. In our case, it can also regulate both pitch and pitch rate within the attraction region for the next cruise flight mode. The terms in (13) are explicitly given below

$$\begin{aligned}\mathbf{x} &= \left(\theta_r, q_r, \int e_\theta dt, \theta, q\right)^T, \\ B &= (0 \ 0 \ 0 \ 0 \ 1)^T \\ A &= \begin{pmatrix} 0 & 1 & 0 & 0 & 0 \\ 0 & 0 & 0 & 0 & 0 \\ 1 & 0 & 0 & -1 & 0 \\ 0 & 0 & 0 & 0 & 1 \\ 0 & 0 & 0 & 0 & 0 \end{pmatrix}, \\ E &= (0 \ 1 \ 0 \ 0 \ 0)^T, \\ C_2 &= (0 \ 0 \ 1 \ 0 \ 0)^T, \\ \mathbf{w} &= \dot{q}_r, \ C_1 = \mathbf{I}(5), \ D_1 = 0, \ D_2 = 0, \ D_{22} = 0.\end{aligned}\quad (16)$$

It can be showed that the RPT control law for the pitch channel can be rewritten as

$$\dot{q}_d = K_{p1} e_\theta + K_{p2} (q_r - q) + K_{p3} \int e_\theta dt \quad (17)$$

where \dot{q}_d is the desired angular acceleration, e_θ is the pitch angle tracking error, q_r is the angular rate reference, and K_{p1} , K_{p2} , and K_{p3} are given by

$$K_{p1} = \frac{\omega_n^2 + 2\zeta\omega_n k_i}{\varepsilon^2}, \ K_{p2} = \frac{2\zeta\omega_n + k_i}{\varepsilon}, \ K_{p3} = \frac{k_i\omega_n^2}{\varepsilon^3} \quad (18)$$

which give a closed-loop characteristic polynomial for the infinite zero structure as

$$p_i(s) = (s + k_i)(s^2 + 2\zeta\omega_n s + \omega_n^2). \quad (19)$$

For J-Lion, we set $\omega_n = 5$, $\zeta = 1$, $\varepsilon = 0.9$, $k_i = 1$.

2) *Roll and Yaw Channels*: The roll and yaw channels are controlled by the usual PID control laws. The roll setpoint is set to be zero, while the yaw setpoint is set with the yaw value when the transition starts. The actuator allocated for the roll channel is the rudder, while fins and ailerons are responsible for the yaw

channel. We set the damping ratio as 0.7 and 0.3 for the roll and yaw channels, respectively, and the natural frequency as 4 rad/s for both. The required PID gains can then be obtained subject to the maximum torque available in each channel.

2) *Backward Transition*: The backward transition adopts the same attitude control method as the forward transition. The difference is that we quicken the maneuver in the pitch channel due to higher dynamics uncertainties compared with the forward transition. The backward transition is designed to be completed within one second. The RPT control parameters are set as $\omega_n = 5$, $\zeta = 1$, $\varepsilon = 0.8$, $k_i = 0.9$ with a slight increase in responsiveness. For the speed channel, the thrust is maintained around the body weight value with vertical velocity feedback. A lower limit of the thrust is also set for safety protection.

C. Cruise Flight Control Design

The cruise flight control design employs a total energy controller for the outer loop to generate the thrust and pitch angle references [42], and an L_1 guidance law for the roll angle reference [43]. The details can be found in [21]. It is vital to point out that our model-based control method in the cruise flight is reflected specifically in the inner loop attitude control. With a sophisticated actuator allocation scheme, attitude stability is ensured under various flight conditions. To illustrate, the fins, elevator, and vectoring thrust propellers are all activated for pitch enhancement. With the model elements in (6), (7), and (8), the required pitch torque can be achieved by the combination of all the three actuators. Note that the inner loop employs almost the same control scheme as in Section IV-A in the kinematic layer except that only yaw rate stabilization is applied.

V. EXPERIMENT RESULTS

A. VTOL Flight Test

We present the VTOL experimental results for J-Lion in this subsection. The mission was to pass a few waypoints fully autonomously. J-Lion took off vertically from the ground with a preset acceleration after the mission was initiated. Fig. 13 depicts the attitude and position tracking performance, velocity response, and IMU acceleration data. The jitters of the yaw angle are caused by the angle constraint $[-\pi, \pi]$. Both the velocity and IMU acceleration are within limited ranges. We should note that the test was carried out with presence of strong wind gust. The high path tracking performance proves that our control system is successful.

B. Full Envelope Flight Test

We have successfully conducted an autonomous full envelope flight including takeoff, VTOL, forward transition, cruise flight, backward transition, and landing. The flight path is shown in Fig. 14. To avoid duplicate description for the VTOL mode, only the transition and cruise flights are illustrated. For visualization convenience, the attitude for the forward transition is expressed in the body frame defined in Section III-A1, while the attitude for the backward transition and cruise flight is expressed in a standard fixed-wing body frame.

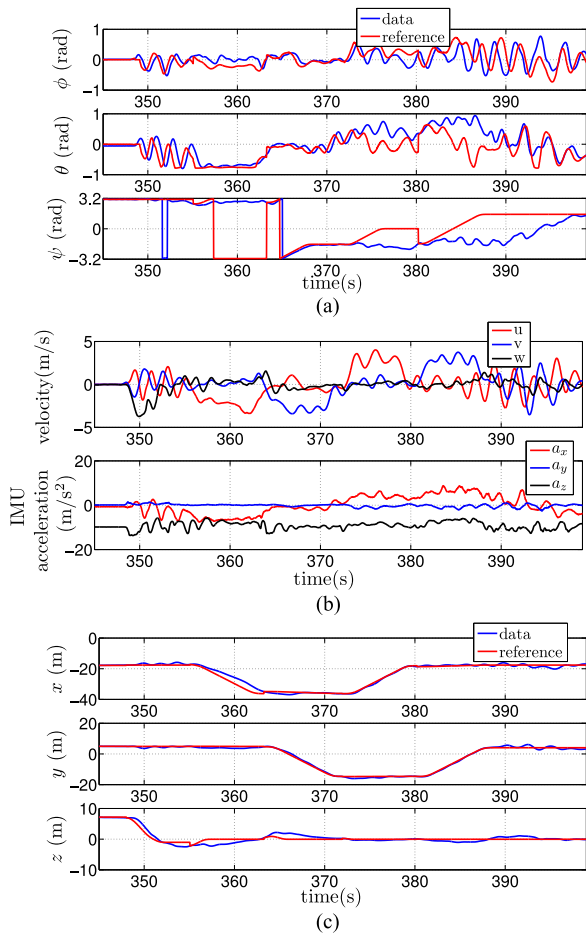


Fig. 13. Outdoor VTOL experiment results. (a) Attitude tracking. (b) Velocity and IMU acceleration data. (c) Position tracking.

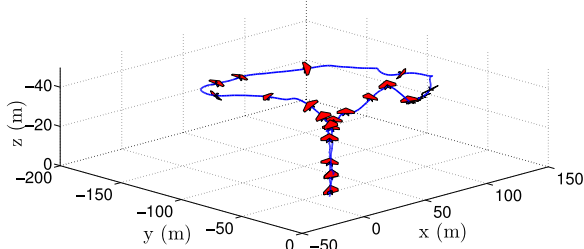


Fig. 14. Flight path in full envelop flight test.

The responses of J-Lion during the forward transition (480.4–483.3 s) are shown in Fig. 15. The airspeed reached 14 m/s for the cruise flight with a steady acceleration. The attitude maintains stability despite wind disturbance and high aerodynamic uncertainties. The pitch channel realizes satisfactory performance due to the robust control design. For the deviation in roll and yaw channels, there are several reasons: i) Lateral wind gust exists during the maneuver; ii) kinetic coupling exists between Euler angles; iii) although the same throttle input is applied for two rotors, any thrust or platform asymmetry can directly lead to angular motion around x_b axis for which the rudder control authority is weak during entry of the transition phase. At current stage, we prioritize the longitudinal stability,

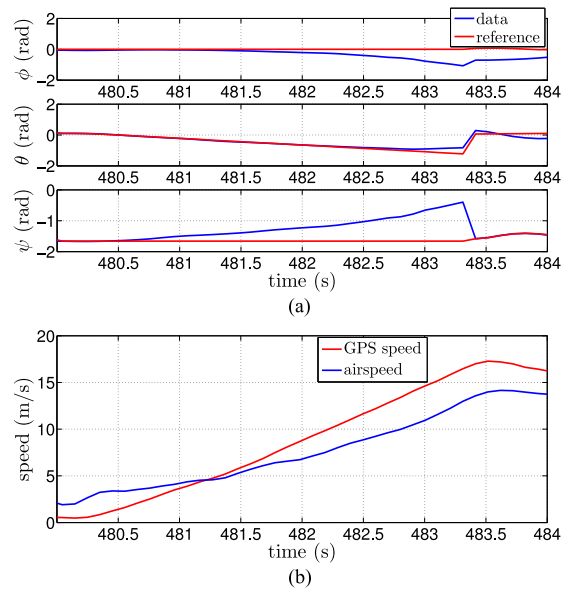


Fig. 15. Responses of J-Lion in forward transition. (a) Attitude tracking. (b) Speed.

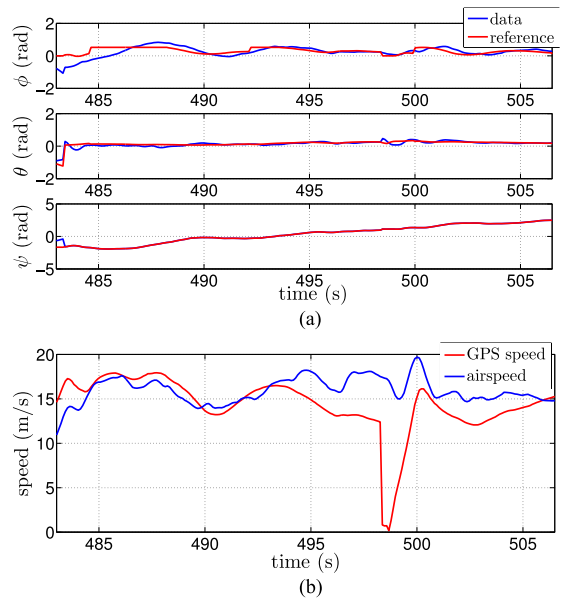


Fig. 16. Responses of J-Lion in cruise flight. (a) Attitude tracking. (b) Speed.

and the differential thrust is not applied during the transition to avoid coupling effect along z_b axis.

For the cruise flight phase in 483.3–506.5 s, the responses of attitude and speed are shown in Fig. 16. J-Lion successfully maintains attitude and cruise speed stability during wind gust. Delayed attitude responses can be foreseen due to aerodynamic torques, and the average cruise speed during test was around 16 m/s.

For the backward transition in 506.6–507 s, the maneuver was finished in 0.5 s with J-Lion responses given in Fig. 17. Due to larger aerodynamic torques resulting from cruise speed, the attitude tracking performance degenerates compared with the forward transition. Nevertheless, the stability of attitude and

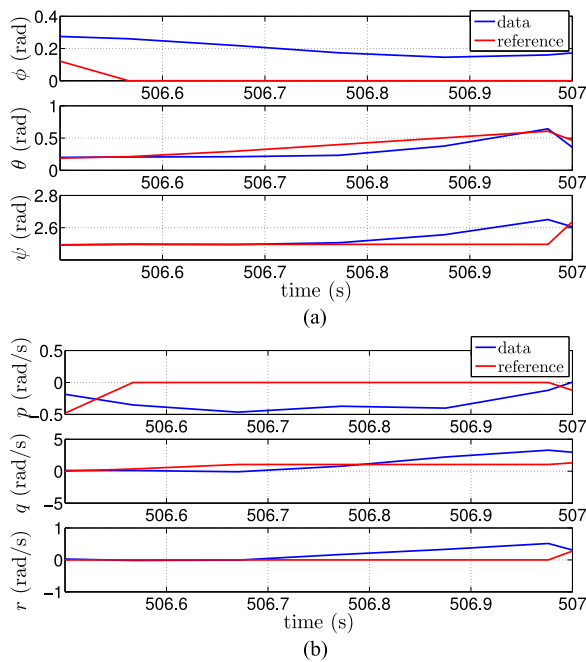


Fig. 17. Responses of J-Lion in backward transition. (a) Attitude tracking. (b) Attitude rate tracking.

attitude rate is also achieved, demonstrating the robustness of our control approach. The height during the maneuver changes little.

The successes of both forward and backward transitions validate our model-based control strategy. Compared with existing attitude tracking data in [27] and our previous work [21], the transition control realizes comparable or better tracking performance in an economic manner.

VI. CONCLUSION

We have presented in this paper, design details for a novel tail-sitter hybrid UAV, J-Lion, with special emphases on the design methodology and aerodynamic design for multiple flight modes. A coherent modeling and control framework comprising essential model elements is synthesized for the full envelope flight. Autonomous VTOL and full envelope flight test results prove our design concept and validate our model-based control method. The video for our flight tests can be found at this web link: <http://uav.ece.nus.edu.sg/JLion2017.mp4>.

REFERENCES

- [1] G. R. Flores, J. Escareo, R. Lozano, and S. Salazar, "Quad-tilting rotor convertible MAV: Modeling and real-time hover flight control," *J. Intell. Robot. Syst.*, vol. 65, no. 1, pp. 457–471, Jan. 2012.
- [2] F. Kendoul, I. Fantoni, and R. Lozano, "Modeling and control of a small autonomous aircraft having two tilting rotors," in *Proc. 44th IEEE Conf. Decis. Control Eur. Control Conf.*, Seville, Spain, 2005, pp. 8144–8149.
- [3] J. H. Lee, B. M. Min, and E. T. Kim, "Autopilot design of tilt-rotor UAV using particle swarm optimization method," in *Proc. IEEE Int. Conf. Control, Autom., Syst.*, Seoul, South Korea, 2007, pp. 1629–1633.
- [4] U. Ozdemir, Y. O. Aktas, K. Demirbag, A. Erdem, G. D. Kalaycoglu, and I. Ozkol, "Design of a commercial hybrid VTOL UAV system," *J. Intell. Robot. Syst.*, vol. 74, no. 1–2, pp. 371–393, Apr. 2014.
- [5] Y. Song and H. Wang, "Design of flight control system for a small unmanned tilt rotor aircraft," *Chin. J. Aeronaut.*, vol. 22, no. 3, pp. 250–256, Jun. 2009.
- [6] E. Cetinsoy *et al.*, "Design and construction of a novel quad tilt-wing UAV," *Mechatronics*, vol. 22, no. 6, pp. 723–745, Sep. 2012.
- [7] K. Muraoka, N. Okada, and D. Kubo, "Quad tilt wing VTOL UAV: Aerodynamic characteristics and prototype flight test," in *Proc. AIAA Infotech@Aerospace Conf.*, Seattle, WA, USA, 2009, pp. 2009–1834.
- [8] J. J. Dickson, D. Miles, O. Cifdalo, V. L. Wells, and A. A. Rodriguez, "Robust LPV H_∞ gain-scheduled hover-to-cruise conversion for a tilt-wing rotorcraft in the presence of CG variations," in *Proc. 46th IEEE Conf. Decis. Control*, New York, NY, USA, 2007, pp. 2773–2778.
- [9] R. H. Stone, "The T-wing tail-sitter unmanned air vehicle: from design concept to research flight vehicle," *J. Aerosp. Eng.*, vol. 218, no. 6, pp. 417–433, Jun. 2004.
- [10] D. Kubo and S. Suzuki, "Tail-sitter vertical takeoff and landing unmanned aerial vehicle: Transitional flight analysis," *J. Aircr.*, vol. 45, no. 1, pp. 292–297, Jan. 2008.
- [11] M. Aksugur and G. Inalhan, "Design methodology of a hybrid propulsion driven electric powered miniature tail-sitter unmanned aerial vehicle," *J. Intell. Robot. Syst.*, vol. 57, no. 1–4, pp. 505–529, Jan. 2010.
- [12] O. Garcia, P. Castillo, K. C. Wong, and R. Lozano, "Attitude stabilization with real-time experiments of a tail-sitter aircraft in horizontal flight," *J. Intell. Robot. Syst.*, vol. 65, no. 1, pp. 123–136, Jan. 2012.
- [13] Google Project Wing. 2014. [Online]. Available: <https://x.company/wing>
- [14] G. Cai, A. Saeed, A. B. Younes, T. Taha, J. Dias, and L. Seneviratne, "First-principles modeling of a miniature tilt-rotor convertiplane in low-speed operation," in *Proc. Int. Micro Air Veh. Conf. Competition*, Beijing, China, 2016, pp. 161–166.
- [15] M. Hochstenbach, C. Notteboom, B. Theys, and D. J. Schutter, "Design and control of an unmanned aerial vehicle for autonomous parcel delivery with transition from vertical take-off to forward flight," *Int. J. Micro Air Veh.*, vol. 7, no. 4, pp. 395–405, Dec. 2015.
- [16] CW-20 VTOL fixed wing UAV. 2017. [Online]. Available: <http://www.jouav.com/index.php/Jouav/index/CW20.html>
- [17] A. K. Kundu, *Aircraft Design*. Cambridge, U.K.: Cambridge Univ. Press, 2010.
- [18] D. P. Raymer, *Aircraft Design: A Conceptual Approach*, 5th ed. Reston, VA, USA: AIAA, 2012.
- [19] M. Aksugur and G. Inalhan, "Design, build, and flight testing of a VTOL tail-sitter unmanned aerial vehicle with hybrid propulsion system," in *Proc. 6th Ankara International Aerospace Conference*, Ankara, Turkey, 2011.
- [20] Wingtra. 2017. [Online]. Available: <https://wingtra.com/product/>
- [21] K. Wang, Y. Ke, and B. M. Chen, "Autonomous reconfigurable hybrid tail-sitter UAV U-Lion," *Sci. China Inf. Sci.*, vol. 60, Mar. 2017, Art. no. 033201.
- [22] R. Bapst, R. Ritz, L. Meier, and M. Pollefeys, "Design and implementation of an unmanned tail-sitter," in *Proc. IEEE/RSSJ Int. Conf. Intell. Robots Syst.*, Hamburg, Germany, 2015, pp. 1885–1890.
- [23] P. Casau, D. Cabecinhas, and C. Silvestre, "Hybrid control strategy for the autonomous transition flight of a fixed-wing aircraft," *IEEE Trans. Control Syst. Technol.*, vol. 21, no. 6, pp. 2194–2211, Nov. 2013.
- [24] A. Banazadeh and N. Taymourtash, "Optimal control of an aerial tail-sitter in transition flight phases," *J. Aircr.*, vol. 53, no. 4, pp. 914–921, Feb. 2016.
- [25] R. Naldi and L. Marconi, "Optimal transition maneuvers for a class of V/STOL aircraft," *Automatica*, vol. 47, no. 5, pp. 870–879, May 2011.
- [26] E. N. Johnson, M. A. Turbe, A. D. Wu, S. K. Kannan, and J. C. Neidhoefer, "Flight test results of autonomous fixed-wing UAV transitions to and from stationary hover," in *Proc. AIAA Guid., Navigat., Control Conf. Exhibit*, Monterey, CA, USA, 2006, pp. 6675–6798.
- [27] S. Verling, B. Weibel, M. Boosfeld, K. Alexis, M. Burri, and R. Siegwart, "Full attitude control of a VTOL tail-sitter UAV," in *Proc. IEEE Int. Conf. Robot. Autom.*, Stockholm, Sweden, 2016, pp. 3006–3012.
- [28] A. Frank, J. McGrew, M. Valenti, D. Levine, and J. P. How, "Hover, transition, and level flight control design for a single-propeller indoor airplane," in *Proc. AIAA Guid., Navigat., Control Conf. Exhibit*, Hilton Head, SC, USA, 2007, pp. 6318–6335.
- [29] H. Ryota and U. Kenji, "Robust design of transition flight control system with input constraint," in *Proc. AIAA Guid., Navigat., Control Conf.*, Kissimmee, FL, USA, 2015, pp. 1768–1778.
- [30] M. S. Selig, J. F. Donovan, and D. B. Fraser, *Airfoils at Low Speeds*. Virginia Beach, VA, USA: SoarTech Publications, 1989.

- [31] M. S. Selig, J. J. Guglielmo, A. P. Broeren, and P. Gigure, *Summary of Low-Speed Airfoil Data*, vol. 1. Virginia Beach, VA, USA: SoarTech Publications, 1995.
- [32] M. S. Selig, C. A. Lyon, P. Gigure, C. N. Ninham, and J. J. Guglielmo, *Summary of Low-Speed Airfoil Data*, vol. 2. Virginia Beach, VA, USA: SoarTech Publications, 1996.
- [33] C. A. Lyon, A. P. Broeren, P. Gigure, A. Gopalarathnam, and M. S. Selig, *Summary of Low-Speed Airfoil Data*, vol. 3. Virginia Beach, VA, USA: SoarTech Publications, 1998.
- [34] J. D. Anderson, *Fundamentals of Aerodynamics*, 5th ed. New York, NY, USA: McGraw-Hill Education, 2010.
- [35] Y. Ke and B. M. Chen, "Full envelope dynamics modeling and simulation for tail-sitter hybrid UAVs," in *Proc. 36th Chin. Control Conf.*, Dalian, China, Jul. 2017, pp. 2242–2247.
- [36] J. Brandt, R. Deters, G. Ananda, and M. Selig, "UIUC propeller database," University of Illinois at Urbana-Champaign. 2015. [Online]. Available: <http://m-selig.ae.illinois.edu/props/propDB.html>
- [37] "APC propeller performance data." 2015. [Online]. Available: <http://www.apcprop.com/Articles.asp?ID=270>
- [38] D. Mellinger and V. Kumar, "Minimum snap trajectory generation and control for quadrotors," in *Proc. IEEE Int. Conf. Robot. Autom.*, Shanghai, China, 2011, pp. 2520–2525.
- [39] L. Meier, P. Tanskanen, F. Fraundorfer, and M. Pollefeys, "Pixhawk: A system for autonomous flight using onboard computer vision," in *Proc. IEEE Int. Conf. Robot. Autom.*, Shanghai, China, 2011, pp. 2992–2997.
- [40] B. M. Chen, *Robust and H_∞ Control*. New York, NY, USA: Springer-Verlag, 2000.
- [41] S. Lai, K. Wang, H. Qin, J. Q. Cui, and B. M. Chen, "A robust online path planning approach in cluttered environments for micro rotorcraft drones," *Control Theory Technol.*, vol. 14, no. 1, pp. 83–96, Feb. 2016.
- [42] A. A. Lambregts, "Vertical flight path and speed control autopilot design using total energy principles," in *Proc. Guid. Control Conf.*, Gatlinburg, TN, USA, 1983, pp. 559–569.
- [43] S. Park, J. Deyst, and J. How, "A new nonlinear guidance logic for trajectory tracking," in *Proc. AIAA Guid., Navigat., Control Conf. Exhibit*, Providence, RI, USA, 2004, pp. 4900–4915.



Yijie Ke received the Bachelor's degree in mechanical engineering from Shanghai Jiao Tong University, Shanghai, China, in 2010, the Master's degree in flight vehicle design from the University of Chinese Academy of Sciences, Beijing, China, in 2013 and the Ph.D degree in electrical and computer engineering from the National University of Singapore, Singapore, in 2017.

His research interests include aircraft design, flight control, aerodynamics, and multidisciplinary design optimization.



Kangli Wang received the B.Eng. and Ph.D. degrees from the Department of Electrical and Computer Engineering, National University of Singapore, Singapore, in 2013 and 2017, respectively.

His main research interests include design and development of hybrid UAVs with vertical takeoff and landing and cruise fly ability and its applications.

Dr. Wang is the recipient of the IEEE Control Systems Chapter (Singapore) Book Prize 2013.



Ben M. Chen received the B.S. degree in mathematics and computer science from Xiamen University, China, in 1983, the M.S. degree in electrical engineering from Gonzaga University, Spokane, Washington, USA, in 1988, and the Ph.D. degree in electrical and computer engineering from Washington State University, Pullman, Washington, USA, in 1991.

He is with the Department of Electrical and Computer Engineering, National University of Singapore, where he is currently a Professor and Provost's Chair. He is also serving as the Director of Control, Intelligent Systems and Robotics Area. His current research interests are in robust control, systems theory, control applications, the development of unmanned systems, and financial market modeling.